Equilibrium Model of Precipitation in Microalloyed Steels

KUN XU, BRIAN G. THOMAS, and RON O'MALLEY

The formation of precipitates during thermal processing of microalloyed steels greatly influences their mechanical properties. Precipitation behavior varies with steel composition and temperature history and can lead to beneficial grain refinement or detrimental transverse surface cracks. This work presents an efficient computational model of equilibrium precipitation of oxides, sulfides, nitrides, and carbides in steels, based on satisfying solubility limits including Wagner interaction between elements, mutual solubility between precipitates, and mass conservation of alloying elements. The model predicts the compositions and amounts of stable precipitates for multicomponent microalloyed steels in liquid, ferrite, and austenite phases at any temperature. The model is first validated by comparing with analytical solutions of simple cases, predictions using the commercial package JMat-PRO, and previous experimental observations. Then it is applied to track the evolution of precipitate amounts during continuous casting of two commercial steels (1004 LCAK and 1006Nb HSLA) at two different casting speeds. This model is easy to modify to incorporate other precipitates, or new thermodynamic data, and is a useful tool for equilibrium precipitation analysis.

I. INTRODUCTION

MICROALLOYED steels are strengthened mainly by the dispersion of fine precipitate particles and their effects to inhibit grain growth and dislocation motion.[1] These precipitates include oxides, sulfides, nitrides, and carbides, and form at different times and locations during steel processing. They display a variety of different morphologies and size distributions, ranging from spherical, cubic to cruciform shape, sizes ranging from nanometers and micrometers and locations inside the matrix or on the grain boundaries, such as shown in Figure 1.[2–6] If properly optimized, these precipitate particles act to pin the grain boundaries, serving to restrict grain growth and thereby increasing toughness during processes such as rolling and run-out table cooling. However, if large numbers of fine precipitate particles accumulate along weak grain boundaries at elevated temperatures, they can lead to crack formation, which plagues processes such as continuous casting.[7] There is a strong need to predict the formation of precipitates, including their composition, morphology, and size distribution, as a function of processing conditions.

Precipitate formation for a given steel composition depends on the temperature history in thermal processes such as casting, and it is accelerated by the strain history in processes with large deformation, such as rolling.[8]

The first crucial step to model precipitate behavior is to predict the equilibrium phases, compositions, and amounts of precipitates present for a given composition and temperature. This represents the maximum amount of precipitate that can form when the solubility limit is exceeded. This is also critical for calculating the supersaturation, which is the driving force for precipitate growth. Thus, a fast and accurate model of equilibrium precipitation is a necessary initial step toward the future development of a comprehensive model of precipitate growth.

Minimization of Gibbs free energy is a popular method to determine the phases present in a multicomponent material at a given temperature. The total Gibbs energy of a multicomponent system is generally described by a regular solution sublattice model.[9,10] In addition to the Gibbs energy of each pure component, extra energy terms come from the entropy of mixing, the excess Gibbs energy of mixing due to interaction between components, and the elastic or magnetic energy stored in the system. In recent years, many researchers have used software packages based on Gibbs energy minimization, including Thermo Calc,[11,12] FactSage,[6] ChemSage,[3] and other CALPHAD models,[13,14] to calculate equilibrium precipitation behavior in multicomponent steels.

Gibbs free energy functions with self-consistent parameters for a Fe-Nb-Ti-C-N steel system have been given by Lee.[14] The carbonitride phase was modeled using a two-sublattice model[15] with (Fe,Nb,Ti)(C,N, Vacancy), where the two sublattices represent the substitutional metal atoms and the interstitial atoms separately. Since not all positions are occupied by interstitial atoms, vacant sites were introduced in this sublattice. Mutual interaction energies between components incorporated up to ternary interactions, and accuracy was confirmed by comparing predictions with thermodynamic properties of Nb/Ti carbonitrides

KUN XU, Graduate Student, and BRIAN G. THOMAS, C.J. Gauthier Professor, are with the Mechanical Science and Engineering Department, University of Illinois at Urbana–Champaign, Urbana, IL, 61801. Contact e-mail: kunxu2@illinois.edu RON O'MALLEY, Plant Metallurgist, is with Nucor Steel Decatur, LLC, Trinity, AL, 35673.
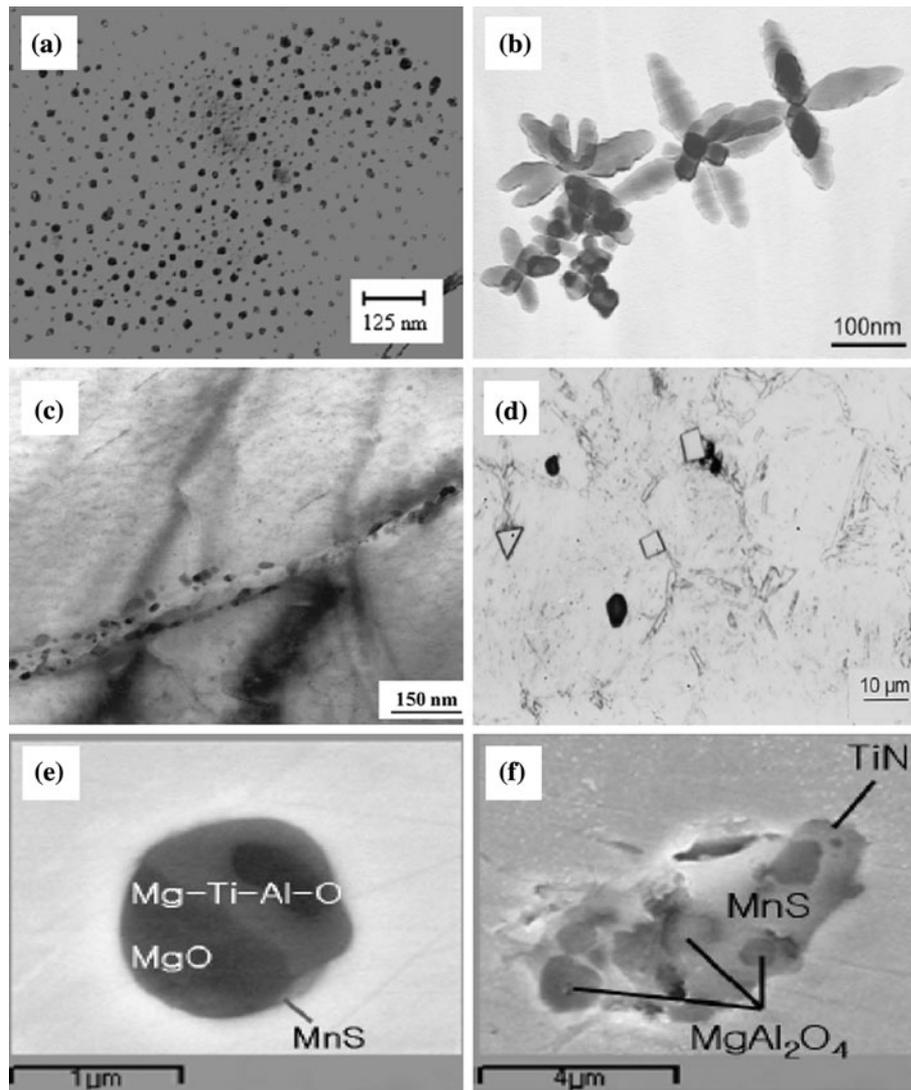
Fig. 1—Example precipitates in microalloyed steels: (a) fine spherical AlN,[2] (b) cruciform (Ti,V)N after equalization at 1373 K (1100 °C),[3] (c) (Ti,Nb)C on grain boundaries,[4] (d) cubic TiN on grain boundaries,[5] and (e) and (f) coarse complex multiple precipitates by heterogeneous nucleation.[6]

measured under equilibrium conditions for a wide range of steel compositions.

Although these models based on minimizing Gibbs free energy can accurately predict the equilibrium amounts of precipitates, and have the powerful ability to predict the precipitates to expect in a new system, the accuracy of their databases and their ability to quantitatively predict complex precipitation of oxides, sulfides, nitrides, and carbides in microalloyed steels is still in question. In addition, the solubility product of each precipitate is a logarithmic function of free energy, so a small inaccuracy in the free energy function could cause a large deviation in calculating the amount precipitated.[16] Finally, the free energy curves and interaction parameters are very interdependent and so must be refit to incorporate new data.

An alternative method to predict the equilibrium phases in a multicomponent alloy is to simultaneously solve systems of equations based on solubility products,

which represent the limits of how much a given precipitate can dissolve per unit mass of metal. The origin of this equilibrium constant concept can be traced back to Le Chatelier's Principle of 1888.[17] The incorporation of mutual solubility was first suggested by Hudd[18] for niobium carbonitride, and later extended by Rose and Gladman[19] to Ti-Nb-C-N steel.

Recently, Liu[20] developed a model to predict the equilibrium mole fractions of precipitates Ti(C,N), MnS, and $Ti_4C_2S_2$ in microalloyed steel. The solubility products are calculated from standard Gibbs energies and account for the interaction between alloying elements and the mutual solubility of Ti(C,N). The precipitation of complex vanadium carbonitrides and aluminum nitrides in C-Al-V-N microalloyed steels was discussed by Gao and Baker.[21] They used two thermodynamic models by Adrian[22] and Rios,[23] and produced similar results. Park[24] calculated the precipitation behavior of MnS in austenite including two

different sets of solubility products for Ti$_4$C$_2$S$_2$ and TiS[11,20] and assuming sulfides and carbonitrides (Ti,V)(C,N) are mutually insoluble. In both works,[21,24] the solution energy of mixing for C-N was assumed to be constant (–4260 J/mol) with all other solution parameters taken as zero. The Wagner interaction effect was neglected for this dilute system and ideal stoichiometry was assumed for all sulfides and carbonitrides.

Previous solubility-product based models often neglect effects such as the differences between substitutional and interstitial elements during precipitation, mutual solubility between precipitates, and the Wagner effect between solutes, so are only suitable for particular steel grades and precipitates. Moreover, the analysis of molten steel and ferrite is lacking as most works only focus on precipitation in the austenite phase.

Although many previous attempts have been made, an accurate model of equilibrium precipitation behavior in microalloyed steel has not yet been demonstrated. The complexity comes from many existing physical mechanisms during precipitation processes, such as solubility limits of precipitates in different steel phases, change of activities due to Wagner interaction between elements, treatment of mutually exclusive and soluble properties among precipitates, and mass conservation of all elements.

The current work aims to establish and apply such a thermodynamic model to efficiently predict the typical precipitates in microalloyed steels. Mutual solubility is incorporated for appropriate precipitates with similar crystal structures and lattice parameters. The model is applied to investigate the effect of mutual solubility. It is then validated with analytical solution of simple cases, numerical results from commercial package JMat-Pro, and previous experimental results. Finally, the model is applied to predict equilibrium precipitation in two commercial microalloyed steels with different casting speeds in practical continuous casting condition.

II. MODEL DESCRIPTION

The equilibrium precipitation model developed in this work computes the composition and amount of each precipitate formed for a given steel composition and temperature, based on satisfying the solubility products of a database of possible reactions and their associated activity interaction parameters. The database currently includes 18 different oxide, sulfide, nitride, and carbide precipitates (TiN, TiC, NbN, NbC$_{0.87}$, VN, V$_4$C$_3$, Al$_2$O$_3$, Ti$_2$O$_3$, MnO, MgO, MnS, MgS, SiO$_2$, TiS, Ti$_4$C$_2$S$_2$, AlN, BN, and Cr$_2$N) and 13 different elements (N, C, O, S, Ti, Nb, V, Al, Mn, Mg, Si, B, and Cr), in Fe, and is easily modified to accommodate new reactions and parameters.

A. Solubility Products

Each reaction between dissolved atoms of elements M and X gives a solid precipitate of compound M$_x$X$_y$:

$$x\mathrm{M} + y\mathrm{X} \leftrightarrow \mathrm{M}_x\mathrm{X}_y \qquad [1]$$

The temperature-dependent equilibrium solubility product, K, is defined as

$$K_{\mathrm{M}_x\mathrm{X}_y} = a_{\mathrm{M}}^x \cdot a_{\mathrm{X}}^y / a_{\mathrm{M}_x\mathrm{X}_y} \qquad [2]$$

where a_{M}, a_{X}, and $a_{\mathrm{M}_x\mathrm{X}_y}$ are the activities of M, X, and M$_x$X$_y$, respectively. The solubility products in steels decrease with lower temperature, so there is usually a critical temperature below which precipitates can form, given sufficient time.

The solubility products of the precipitates in liquid steel, ferrite, and austenite used in this study are listed in Table I. The solubilities in liquid are about 10 to 100 times larger than those in austenite, which are about 10 times greater than those in ferrite at the same temperature. These observed ratios are assumed to estimate unknown solubility products for oxides in solid steel and for the other precipitates in liquid steel. The solubility products generally decrease from carbides, to nitrides, to sulfides, to oxides, which corresponds to increasing precipitate stability. Thus, oxides generally precipitate first, forming completely in the liquid steel, where they may collide and grow very large, leaving coarse oxide particles (inclusions) and very little free (dissolved) oxygen remaining in the solid phase after solidification. In addition, oxide precipitates in the solid often act as heterogeneous nucleation cores of complex precipitates, which form later at lower temperature.[63,64]

The solubilities and amounts of nitrides and carbides added to microalloyed steels typically result in these precipitates forming in the austenite phase as small (nanometer-scale) second-phase particles, which inhibit grain growth. A notable precipitate is TiN, which is roughly 100 to 1000 times more stable than other nitrides and carbides. The large variations between the ratio of carbide and nitride solubility products also depend greatly on the alloying elements. This ratio is about 10 for niobium, so NbC$_{0.87}$ precipitates are commonly observed in steels because carbon is always relatively plentiful. This ratio is about 100 to 1000 for titanium and vanadium, so these elements typically precipitate as nitrides. When the concentration of sulfur is high enough, the corresponding sulfides and carbosulfides are also observed in these steels.

For the low solute contents of the steels, the activity a_i of each element i (weight percent) is defined using Henry's law as follows:

$$a_i = \gamma_i[\mathrm{pct\ i}]$$

where

$$\log_{10} \gamma_i = \sum_{j=1}^{13} e_i^j [\mathrm{pct\ j}] \qquad [3]$$

where γ_i is the activity coefficient, e_i^j is the Wagner interaction coefficient of element i as affected by alloying element j, and [pct i] is the dissolved mass concentration of element i (wt pct). The summation covers interactions from all alloying elements, including element i itself. This relation comes from the Taylor series expansion formalism first proposed by Wagner[65]

Table I. Lattice Parameters and Solubility Products of Precipitates

Composition (Mass Pct)	Crystal Form Lattice Parameter	$\text{Log}_{10}K_l$	$\text{Log}_{10}K_{\alpha,\delta}$	$\text{Log}_{10}K_{\gamma}$
Al_2O_3 [pct Al]^2[pct O]^3	hexagonal[25] $a = 4.76$Å, $c = 13.0$Å	$-\frac{64,000}{T} + 20.57$[33]	$-\frac{51,630}{T} + 7.55^*$	$-\frac{51,630}{T} + 9.45$[38]
Ti_2O_3 [pct Ti]^2[pct O]^3	hexagonal[26] $a = 5.16$Å, $c = 13.6$Å	$-\frac{56060}{T} + 18.08$[34]	$-\frac{56060}{T} + 14.08^*$	$-\frac{56060}{T} + 15.98^*$
MgO [pct Mg][pct O]	fcc[25] $a = 4.21$Å	$-\frac{4700}{T} - 4.28$[35]	$-\frac{4700}{T} - 6.28^*$	$-\frac{4700}{T} - 5.33^*$
MnO [pct Mn][pct O]	fcc[27] $a = 4.45$Å	$-\frac{11749}{T} + 4.666$[36]	$-\frac{11749}{T} + 2.666^*$	$-\frac{11749}{T} + 3.616^*$
SiO_2 [pct Si][pct O]^2	trigonal[28] $a = 4.91$Å, $c = 5.41$Å	$-\frac{30,110}{T} + 11.40$[33]	$-\frac{30,110}{T} + 9.40^*$	$-\frac{30,110}{T} + 10.35^*$
MnS [pct Mn][pct S]	fcc[29] $a = 5.22$Å	$-\frac{9020}{T} + 3.98^*$	$-\frac{9020}{T} + 1.98^*$	$-\frac{9020}{T} + 2.93$[39]
MgS [pct Mg][pct S]	fcc[29] $a = 5.20$Å	$-\frac{9268}{T} + 2.06^*$	$-\frac{9268}{T} + 0.06^*$	$-\frac{9268}{T} + 1.01$[40]
TiS [pct Ti][pct S]	trigonal[30] $a = 3.30$Å, $c = 26.5$Å	$-\frac{13,975}{T} + 6.48^*$	$-\frac{13,975}{T} + 4.48^*$	$-\frac{13,975}{T} + 5.43$[41]
$Ti_4C_2S_2^{**}$ [pct Ti]^4[pct C]^2[pct S]^2	hexagonal[30] $a = 3.30$Å, $c = 11.2$Å	$-\frac{68,180}{T} + 35.8^*$	$-\frac{68,180}{T} + 27.8^*$	$-\frac{68,180}{T} + 31.6$[41]
AlN [pct Al][pct N]	hexagonal[19] $a = 3.11$Å, $c = 4.97$Å	$-\frac{12,950}{T} + 5.58$[37]	$-\frac{8790}{T} + 2.05$[37]	$-\frac{6770}{T} + 1.03$[37]
BN [pct B][pct N]	hexagonal[31] $a = 2.50$Å, $c = 6.66$Å	$-\frac{10,030}{T} + 4.64$[37]	$-\frac{14,250}{T} + 4.61$[37]	$-\frac{13,970}{T} + 5.24$[37]
NbN [pct Nb][pct N]	fcc[19] $a = 4.39$Å	$-\frac{12,170}{T} + 6.91^*$	$-\frac{12,170}{T} + 4.91$[37]	$-\frac{10,150}{T} + 3.79$[37]
$NbC_{0.87}$ [pct Nb][pct C]$^{0.87}$	fcc[19] $a = 4.46$Å	$-\frac{9830}{T} + 6.33^*$	$-\frac{9830}{T} + 4.33$[37]	$-\frac{7020}{T} + 2.81$[37]
TiN [pct Ti][pct N]	fcc[19] $a = 4.23$Å	$-\frac{17,040}{T} + 6.40$[37]	$-\frac{18,420}{T} + 6.40$[37]	$-\frac{15,790}{T} + 5.40$[37]
TiC [pct Ti][pct C]	fcc[19] $a = 4.31$Å	$-\frac{6160}{T} + 3.25$[37]	$-\frac{10,230}{T} + 4.45$[37]	$-\frac{7000}{T} + 2.75$[37]
VN [pct V][pct N]	fcc[19] $a = 4.12$Å	$-\frac{9720}{T} + 5.90^*$	$-\frac{9720}{T} + 3.90$[37]	$-\frac{7700}{T} + 2.86$[37]
$V_4C_3^{**}$ [pct V]^4[pct C]^3	fcc[19] $a = 4.15$Å	$-\frac{28,200}{T} + 24.96^*$	$-\frac{28,200}{T} + 16.96$[37]	$-\frac{26,240}{T} + 17.8$[37]
Cr_2N [pct Cr]^2 [pct N]	trigonal[32] $a = 4.76$Å, $c = 4.44$Å	$-\frac{1092}{T} - 0.131^*$	$-\frac{1092}{T} - 2.131^*$	$-\frac{1092}{T} - 1.181$[42]

*Estimated values used in the present work; temperature is in Kelvin.
**For consistency, these solubility products are rewritten in the form M_xX_y, according to $\log_{10} K_{M_xX_y} = x \log_{10} K_{MX_{y/x}}$.

and Chipman[66] to describe the thermodynamic relationship between logarithm of activity coefficient and composition of a dilute constituent in a multicomponent system. Larger positive Wagner interaction parameters encourage more precipitation. If the alloying concentrations are higher, then higher-order interaction coefficients using the extended treatment by Lupis and Elliott[67] should be used. Since alloy additions are small in the microalloyed steels of interest in this work (<~1 wt pct), they are assumed to be dilute, so only first-order interaction coefficients were collected. Relative to the solubility product effects, these interaction parameters are a second-order correction to precipitation in these steels. Each referenced value was determined in either the liquid melt or solid steel. They are assumed independent of steel phase and are summarized in Table II.

During phase transformations, when the steel has more than one phase (liquid, δ-ferrite, austenite, and α-ferrite), the solubility product of the precipitate M_xX_y is defined with a weighted average based on the phase fractions as follows:

$$K_{M_xX_y} = f_l \cdot K_{M_xX_y}^l + f_\delta \cdot K_{M_xX_y}^\delta + f_\gamma \cdot K_{M_xX_y}^\gamma + f_\alpha \cdot K_{M_xX_y}^\alpha \quad [4]$$

where f_l, f_δ, f_γ, and f_α are the phase fractions of liquid, δ-ferrite, austenite, and α-ferrite in steel.

B. Treatment of Mutual Solubility

Although many different precipitates are included in the previous section, several groups are mutually soluble, as they exist as a single constituent phase. There is ample experimental evidence to show the mutual solubility of (Ti,Nb,V)(C,N) carbonitride in steels. The treatment of mutual solubility follows the ideas of Huud,[18] Gladman,[19] and Speer[68] et al., and assumes ideal mixing (regular solution parameters are zero) for mutually soluble precipitates. The activities of precipitates that are mutually exclusive with each other remain at unity

Table II. Selected Interaction Coefficients in Dilute Solutions of Microalloyed Steel

Element j	e_N^i	e_C^i	e_S^i	e_O^i	e_{Ti}^i	e_{Nb}^i
N	6294/T[43]	5790/T[46]	0.007[37]	0.057[50]	−19,500/T + 8.37[47]	—
C	0.06[37]	8890/T[44]	0.11[37]	−0.42[33]	−221/T − 0.072[33]	—
S	0.007[37]	0.046[37]	−8740/T − 0.394[45]	−0.133[50]	−0.27[33]	—
O	0.05[37]	−0.34[37]	−0.27[37]	−1750/T + 0.76[33] −3.4[33]	−1.12[33]	—
Ti	−5700/T + 2.45[47]	−55/T − 0.015[33]	−0.072[50]	−1.12[33]	0.042[33]	—
Nb	−235/T + 0.055[48]	−66,257/T[54]	—	—	—	−2[46]
V	−356/T + 0.0973[49]	—	—	—	—	—
Al	−0.028[50]	0.043[37]	0.035[50]	−1.17[33]	0.93[58]	—
Mn	−8336/T − 27.8 + 3.652 ln T[51]	−5070/T[55]	−0.026[37]	−0.021[33]	−0.043[33]	—
Mg	—	−0.07[50]	—	−1.98[33]	−1.01[59]	—
Si	−286/T + 0.202[52]	162/T − 0.008[50]	0.063[37]	−0.066[33]	177.5/T − 0.12[52]	77265/T − 44.9[54]
B	1000/T − 0.437[53]	—	—	—	—	—
Cr	−65,150/T + 24.1[51]	−21,880/T + 7.02[56]	−0.011[50]	−0.046[57]	−0.016[57]	−216,135/T + 140.8[54]

Element j	e_V^i	e_{Al}^i	e_{Mn}^i	e_{Mg}^i	e_{Si}^i	e_B^i	e_{Cr}^i
N	—	−0.058[50]	—	—	—	—	—
C	—	0.091[33]	−0.0538[33]	−0.25[59]	0.18[33]	—	−0.12[50]
S	—	0.035[33]	−28418/T + 12.8[39]	—	0.066[33]	—	−153/T + 0.062[50]
O	—	−1.98[33]	−0.083[33]	−3[33]	−0.119[33]	—	−0.14[50]
Ti	—	0.004[58]	−0.05[33]	−0.51[59]	1.23[33]	—	0.059[50]
Nb	—	—	—	—	—	—	—
V	470/T−0.22[60]	—	—	—	—	—	—
Al	—	0.043[33]	0.027[61]	−0.12[59]	0.058[33]	—	0.023[57]
Mn	—	0.035[61]	−175.6/T + 2.406[43]	—	−0.0146[33]	—	0.0039[33]
Mg	—	−0.13[59]	—	—	—	—	0.042[62]
Si	—	0.056[33]	−0.0327[33]	−0.088[33]	0.103[33]	—	−0.0043[50]
B	—	—	—	—	—	0.038[53]	—
Cr	—	0.012[57]	0.0039[33]	0.047[59]	−0.0003[33]	—	−0.0003[50]

—: Values not found in the literature; they are assumed to be zero in current calculation.

because they exist separately in the steel. On the other hand, the activities of mutually soluble precipitates are less than unity because they always appear together with other precipitates. Instead, their activities are represented by their respective molar fractions in the mixed precipitates, so the sum of the activities of the precipitates that comprise a mutually soluble group is unity. The crystal structures and lattice parameters of the precipitates are given in Table I. Precipitates with the same crystal structures and similar lattice parameters (within 10 pct) are assumed to be mutually soluble, and this assumption could be adjusted by further experimental observations.

According to the preceding criterion, the 18 precipitates in the current work are separated into the following 10 groups: (Ti,Nb,V)(C,N), (Al,Ti)O, (Mn,Mg)O, (Mn,Mg)S, SiO_2, TiS, $Ti_4C_2S_2$, AlN, BN, and Cr_2N. Precipitates can form from the element combinations that comprise each of these groups, including those for the four mutually soluble groups shown in Table III. The 18 solubility limits provide the following constraint equation:

$$a_{M_xX_y} = \frac{a_M^x \cdot a_X^y}{K_{M_xX_y}} \qquad [5]$$

The activity of precipitate M_xX_y, $a_{M_xX_y}$, is determined differently for mutually soluble and exclusive

Table III. Mutually soluble Precipitate Groups and Their Precipitates

Mutually soluble Precipitate Group	Precipitate Types Involved
(Ti,Nb,V)(C,N)	TiN, NbN, VN, TiC, $NbC_{0.87}$, V_4C_3,
(Al,Ti)O	Al_2O_3, Ti_2O_3
(Mn,Mg)O	MnO, MgO
(Mn,Mg)S	MnS, MgS

precipitates. Its value is 1 for the six mutually exclusive precipitates (SiO_2, TiS, $Ti_4C_2S_2$, AlN, BN, and Cr_2N). For the four mutually soluble precipitate groups, the precipitate activities must satisfy

$$a_{TiN} + a_{NbN} + a_{VN} + a_{TiC} + a_{NbC_{0.87}} + a_{V_4C_3} = 1 \qquad [6]$$

$$a_{Al_2O_3} + a_{Ti_2O_3} = 1 \qquad [7]$$

$$a_{MnO} + a_{MgO} = 1 \qquad [8]$$

$$a_{MnS} + a_{MgS} = 1 \qquad [9]$$

The y/x ratio of each precipitate M_xX_y is easily calculated from Table I and is often a nonstoichiometric

Table IV. Precipitates Considered for Each Alloying-Element Mass Balance

Element	Groups of Precipitates	Types of Precipitates
N	(Ti,Nb,V)(C,N), AlN, BN, Cr_2N	TiN, NbN, VN, AlN, BN, Cr_2N
C	(Ti,Nb,V)(C,N), $Ti_4C_2S_2$	TiC, $NbC_{0.87}$, V_4C_3, $Ti_4C_2S_2$
S	(Mn,Mg)S, TiS, $Ti_4C_2S_2$	MnS, MgS, TiS, $Ti_4C_2S_2$
O	(Al,Ti)O, (Mn,Mg)O, SiO_2	Al_2O_3, Ti_2O_3, MnO, MgO, SiO_2
Ti	(Ti,Nb,V)(C,N), (Al,Ti)O, TiS, $Ti_4C_2S_2$	TiN, TiC, Ti_2O_3, TiS, $Ti_4C_2S_2$
Nb	(Ti,Nb,V)(C,N)	NbN, $NbC_{0.87}$
V	(Ti,Nb,V)(C,N)	VN, V_4C_3
Al	(Al,Ti)O, AlN	Al_2O_3, AlN
Mn	(Mn,Mg)O, (Mn,Mg)S	MnO, MnS
Mg	(Mn,Mg)O, (Mn,Mg)S	MgO, MgS
Si	SiO_2	SiO_2
B	BN	BN
Cr	Cr_2N	Cr_2N

fraction, according to experimental observations. With wide uncertainties in measured solubility products,[19] further research is needed to modify these data to best match new measurements.

C. *Mass Balance on Alloying Elements*

The total of the molar fractions of each group of precipitates in the steel is

$$\chi_{total} = \chi_{(Ti,Nb,V)(C,N)} + \chi_{(Al,Ti)O} + \chi_{(Mn,Mg)O} + \chi_{(Mn,Mg)S}$$
$$+ \chi_{SiO_2} + \chi_{TiS} + \chi_{Ti_4C_2S_2} + \chi_{AlN} + \chi_{BN} + \chi_{Cr_2N} \quad [10]$$

The following equations must be satisfied for the mass balance of each of the 13 alloying elements, by summing over all 18 precipitate types, as summarized in Table IV:

$$\chi_{M_0} = (1 - \chi_{total})\chi_{[M]} + \sum_{i=1}^{18} \left(x\chi_{M_xX_y} \right)_i \quad [11]$$

$$\chi_{X_0} = (1 - \chi_{total})\chi_{[X]} + \sum_{i=1}^{18} \left(y\chi_{M_xX_y} \right)_i \quad [12]$$

where $\chi_{M_0} = A_{steel}M_0/(100A_M)$ and $\chi_{[M]} = A_{steel}[M]/(100A_M)$ are the molar fractions of the total mass concentration, M_0 (wt pct), of the given element in the steel composition and the dissolved concentration [M] (wt pct) for the element M. A_{steel} and A_M are the atomic mass of the steel matrix and element M. A similar relation holds for element X in Eq. [12]. The relation indicates that the total concentration of each alloying element is divided into that in solution and that in precipitate form. The molar fraction $\chi_{M_xX_y}$ of precipitate M_xX_y is the product of the activity of this precipitate and its corresponding molar fraction of the precipitate group

$$\chi_{M_xX_y} = a_{M_xX_y}\chi_g \quad [13]$$

where χ_g is the molar fraction of mutually soluble precipitate group g, which contains precipitate M_xX_y. For example, the group g = (Ti,Nb,V)(C,N) contains

M_xX_y precipitates TiN, NbN, VN, TiC, $NbC_{0.87}$, or V_4C_3.

Generally, there are **P** equations for the solubility limits of **P** precipitates, **M** equations for the mass balances of **M** alloying elements, and **Q** extra constraint equations for the **Q** groups of mutually soluble precipitates. The total number of equations is **P + M + Q**. In addition, there are **M** unknown dissolved concentrations of the **M** alloying elements, **R** molar concentrations of the **R** groups of mutually exclusive precipitates, **Q** molar concentrations of the **Q** groups of mutually soluble precipitates, and **P − R** mutually soluble coefficients. Thus, the total number of unknowns is also **M + Q + P**. The current study includes **P = 18** precipitates, **M = 13** alloying elements, and **Q = 4** mutually soluble groups, giving **35** equations and **35** unknowns. With an equal number of equations and unknowns, the equation system can be solved by suitable numerical method.

D. *Numerical Solution Details*

The preceding equations are solved simultaneously using a simple iterative scheme. To achieve faster convergence, the method takes advantage of the fact that results are desired over a wide temperature range, as it runs incrementally from above the solidus temperature to below the austenite to α-ferrite transformation temperature. Starting at a high temperature in liquid steel, complete solubility of every precipitate phase is assumed. The temperature is lowered at each time-step, using the results from the previous step as the initial guess. The 35 equations are solved using the Newton–Raphson method until the largest absolute error between the left and right sides of all equations converges to less than 10^{-6}. The (35×35) matrix of the derivatives of the equations with respect to the unknowns is calculated analytically. The solution of this system of equations F_i is given as

$$z_{k+1} = z_k - \lambda J(z_k)^{-1}F(z_k) \quad [14]$$

The Jacobian matrix **J** is computed from

$$\{J(z)\}_{ij} = \frac{\partial F_i(z)}{\partial z_j} \quad [15]$$

The parameter λ is continuously halved from unity until the norm of the equations system decreases. After solving the equations, the dissolved concentrations of each alloying element and the amounts of each precipitate formed are stored at each temperature. It is worth mentioning that the computational time is typically smaller than 0.1 seconds for each temperature, so the current model gives a relatively quick prediction of the equilibrium phases for microalloyed steels. Such an efficient model is needed for coupling into a kinetic model in future work.

The stoichiometry requirement for this chemical reaction is

$$\frac{Nb_0 - [Nb]}{A_{Nb}} = \frac{N_0 - [N]}{A_N} \quad [19]$$

The analytical solution can be summarized as follows.

(a) At high temperature, when $Nb_0 * N_0 \leq K_{NbN}$, there are no precipitates.
(b) At lower temperature, when $Nb_0 * N_0 > K_{NbN}$,

$$[N] = \frac{(A_{Nb}N_0 - A_N Nb_0) + \sqrt{(A_{Nb}N_0 - A_N Nb_0)^2 + 4A_{Nb}A_N K_{NbN}}}{2A_{Nb}}$$

$$[Nb] = \frac{-(A_{Nb}N_0 - A_N Nb_0) + \sqrt{(A_{Nb}N_0 - A_N Nb_0)^2 + 4A_{Nb}A_N K_{NbN}}}{2A_N} \quad [20]$$

$$w_{NbN} = (A_{Nb} + A_N)\left(\frac{(A_{Nb}N_0 + A_N Nb_0) - \sqrt{(A_{Nb}N_0 - A_N Nb_0)^2 + 4A_{Nb}A_N K_{NbN}}}{2A_{Nb}A_N}\right)$$

The molar concentration of precipitate can be transformed to the mass concentration or volume fraction in steels. For precipitate M_xX_y, its mass concentration $w_{M_xX_y}$ (wt pct) and volume fraction $v_{M_xX_y}$ are calculated from its molar fraction $\chi_{M_xX_y}$, as follows:

$$w_{M_xX_y} = \frac{100A_{M_xX_y}\chi_{M_xX_y}}{A_{steel}} \quad [16]$$

$$v_{M_xX_y} = \frac{\rho_{steel}A_{M_xX_y}}{\rho_{M_xX_y}A_{steel}}\chi_{M_xX_y} \quad [17]$$

where A_{steel} and $A_{M_xX_y}$ are the atomic mass, and ρ_{steel} and $\rho_{M_xX_y}$ are the density of the steel matrix and precipitate separately. As the alloy additions are small, these properties of steel are simply taken to be constants (55.85 g/mol and 7500 kg/m^3).

III. INFLUENCE OF MUTUAL SOLUBILITY ON PRECIPITATION

A. Validation with Analytical Solutions of Mutually Exclusive Precipitates

For simple single-precipitate systems with $y/x = 1$, such as NbN, Wagner interaction can be neglected and the element activities are equal to their dissolved mass concentration in the very dilute systems. The first precipitate occurs when the product of the initial concentrations, Nb_0 and N_0, exceeds K_{NbN}. After NbN forms, the solubility limit requires

$$[Nb][N] = K_{NbN} \quad [18]$$

For mutually exclusive precipitates composed with $y/x = 1$, if these precipitates do not share any alloying elements, the analytical solution is simply two sets of equations such as those for NbN. Alternatively, if they share a common element, such as with the Nb-Al-N system with NbN and AlN, all of the different possible conditions, such as $Nb_0 * N_0 > K_{NbN}$ and $Al_0 * N_0 > K_{AlN}$, are tested to find which precipitate forms first. After one precipitate forms, the initial nitrogen concentration is replaced with its dissolved value to judge whether the other precipitate forms or not and the results change if both precipitates form.

If both precipitates form, the solubility limits and chemical reaction require

$$[Nb][N] = K_{NbN} \quad [21]$$

$$[Al][N] = K_{AlN} \quad [22]$$

$$\frac{Nb_0 - [Nb]}{A_{Nb}} + \frac{Al_0 - [Al]}{A_{Al}} = \frac{N_0 - [N]}{A_N} \quad [23]$$

The solution can be summarized as follows.

(a) At high temperature, when $Nb_0 * N_0 \leq K_{NbN}$ and $Al_0 * N_0 \leq K_{AlN}$, there is no precipitate.
(b) At low temperature, when either $Nb_0 * N_0 > K_{NbN}$ and $Al_0 * N_0 > K_{AlN}$ is satisfied:

  (i) If $Nb_0 * N_0 > K_{NbN}$, the solution is given like a single NbN case
  (ii) If $Al_0 * N_0 > K_{AlN}$, the solution is similar to Eq. [20], but all values of Nb are replaced with the corresponding values of Al instead.

(c) If the temperature continues to decrease so that both $Nb_0*N_0 > K_{NbN}$ and $Al_0*N_0 > K_{AlN}$ are satisfied, Nb_0*N_0/K_{NbN} and Al_0*N_0/K_{AlN} are computed and compared

(i) If Nb_0*N_0/K_{NbN} is larger, the following condition is checked

$$Al_0 * [N] > K_{AlN} \qquad [24]$$

If true, then both precipitates form. Otherwise, only NbN precipitates exist.

(ii) If Al_0*N_0/K_{AlN} is larger, the next condition is checked:

$$Nb_0 * [N] > K_{NbN} \qquad [25]$$

If true, then both precipitates form. Otherwise, only AlN precipitates exist.

(iii) If both precipitates form,

very well for all three hypothetical steels. By adding 0.02 pct Al into steel with 0.02 pct Nb and 0.02 pct N, AlN forms first, consumes some of the dissolved nitrogen, which delays the formation of NbN precipitate, and decreases the equilibrium amount of NbN. Instead, if 0.01 pct B is added to the 0.02 pct Nb and 0.02 pct N steel, the early precipitation of BN delays NbN to form at an even lower temperature. This is because BN has a lower solubility limit and reacts with more nitrogen in forming BN because of the lower atomic mass of boron.

A precipitation diagram for the Nb-Al-N-Fe system at different temperatures in austenite was calculated from the current model and is shown in Figure 3. The sum of the mass concentration of elements Nb, Al, and N is set as 0.05 wt pct. Each curve in this diagram shows the boundary between stable and unstable precipitation of AlN or NbN in these hypothetical steels. At 1573 K (1300 °C), AlN forms first because of its lower solubility

$$[N] = \frac{[A_{Nb}A_{Al}N_0 - A_N(A_{Nb}Al_0 + A_{Al}Nb_0)]}{2A_{Nb}A_{Al}}$$
$$+ \frac{\sqrt{[A_{Nb}A_{Al}N_0 - A_N(A_{Nb}Al_0 + A_{Al}Nb_0)]^2 + 4A_{Nb}A_{Al}A_N(A_{Nb}K_{AlN} + A_{Al}K_{NbN})}}{2A_{Nb}A_{Al}}$$

$$[Nb] = \frac{-K_{NbN}[A_{Nb}A_{Al}N_0 - A_N(A_{Nb}Al_0 + A_{Al}Nb_0)]}{2A_N(A_{Nb}K_{AlN} + A_{Al}K_{NbN})}$$
$$+ \frac{K_{NbN}\sqrt{[A_{Nb}A_{Al}N_0 - A_N(A_{Nb}Al_0 + A_{Al}Nb_0)]^2 + 4A_{Nb}A_{Al}A_N(A_{Nb}K_{AlN} + A_{Al}K_{NbN})}}{2A_N(A_{Nb}K_{AlN} + A_{Al}K_{NbN})}$$

$$[Al] = \frac{-K_{AlN}[A_{Nb}A_{Al}N_0 - A_N(A_{Nb}Al_0 + A_{Al}Nb_0)]}{2A_N(A_{Nb}K_{AlN} + A_{Al}K_{NbN})}$$
$$+ \frac{K_{AlN}\sqrt{[A_{Nb}A_{Al}N_0 - A_N(A_{Nb}Al_0 + A_{Al}Nb_0)]^2 + 4A_{Nb}A_{Al}A_N(A_{Nb}K_{AlN} + A_{Al}K_{NbN})}}{2A_N(A_{Nb}K_{AlN} + A_{Al}K_{NbN})} \qquad [26]$$

$$w_{NbN} = (A_{Nb} + A_N)\left[\frac{K_{NbN}(A_{Nb}A_{Al}N_0 + A_N(A_{Al}Nb_0 - A_{Nb}Al_0)) + 2A_{Nb}A_N Nb_0 K_{AlN}}{2A_{Nb}A_N(A_{Nb}K_{AlN} + A_{Al}K_{NbN})}\right.$$
$$\left. - \frac{K_{NbN}\sqrt{[A_{Nb}A_{Al}N_0 - A_N(A_{Nb}Al_0 + A_{Al}Nb_0)]^2 + 4A_{Nb}A_{Al}A_N(A_{Nb}K_{AlN} + A_{Al}K_{NbN})}}{2A_{Nb}A_N(A_{Nb}K_{AlN} + A_{Al}K_{NbN})}\right]$$

$$w_{AlN} = (A_{Al} + A_N)\left[\frac{K_{AlN}(A_{Nb}A_{Al}N_0 + A_N(A_{Nb}Al_0 - A_{Al}Nb_0)) + 2A_{Al}A_N Al_0 K_{NbN}}{2A_{Al}A_N(A_{Nb}K_{AlN} + A_{Al}K_{NbN})}\right.$$
$$\left. - \frac{K_{AlN}\sqrt{[A_{Nb}A_{Al}N_0 - A_N(A_{Nb}Al_0 + A_{Al}Nb_0)]^2 + 4A_{Nb}A_{Al}A_N(A_{Nb}K_{AlN} + A_{Al}K_{NbN})}}{2A_{Al}A_N(A_{Nb}K_{AlN} + A_{Al}K_{NbN})}\right]$$

For mutually-exclusive precipitates, which share alloying elements, the formation of the first precipitate phase changes the dissolved concentration of shared elements and delays the formation of other precipitates. The interaction parameters are all set to zero for numerical simulation of these test cases. Figure 2 shows that the numerical results match the analytical solution

limit. The composition region for stable AlN precipitation increases with decreasing temperature. When temperature drops below 1423 K (1150 °C), either AlN or NbN may exist for certain compositions. Finally, at temperatures below 1398 K (1125 °C), either AlN, NbN, or both precipitates can coexist. Similar progressions occur in other systems.
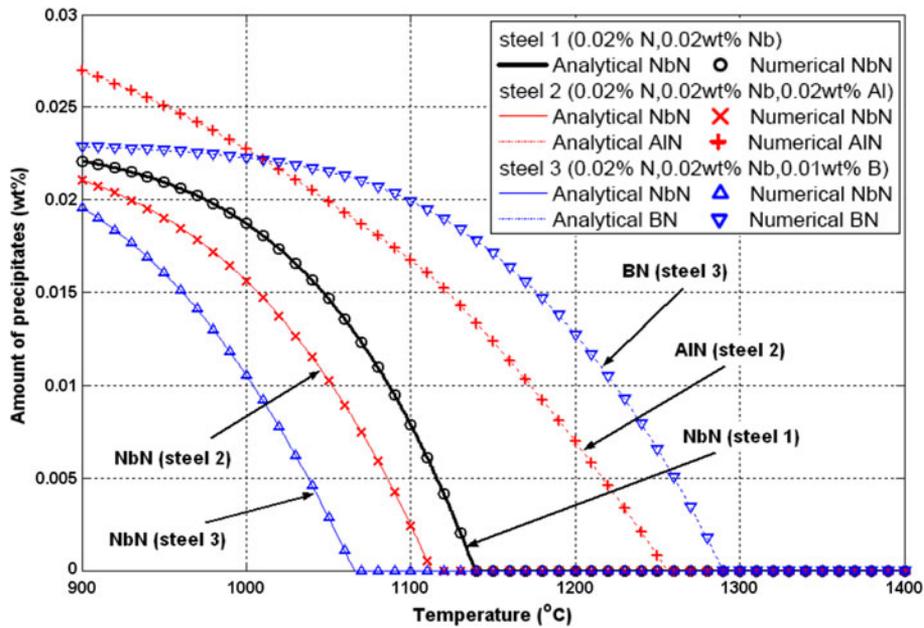
Fig. 2—Comparison of mutually-exclusive precipitation model predictions with analytical solution in austenite for three Fe alloys containing 0.02 pct N and 0.02 pct Nb and either 0.02 pct Al or 0.01 pct B.
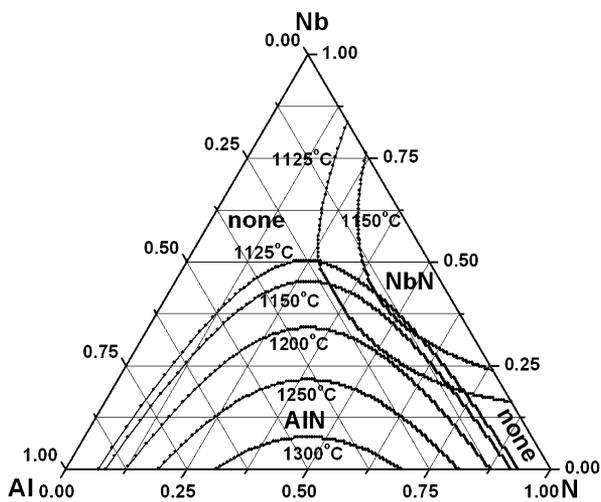

Fig. 3—Calculated precipitation phase diagram for the quaternary Nb-Al-N system with 99.95 pct Fe.

B. Calculation for Mutually Soluble Precipitates

A prediction of mutually soluble precipitation is shown in Figure 4 for a hypothetical Ti-Nb-N steel with 0.01 pct Nb, 0.01 pct N, and 0.005 pct Ti. The precipitates form as the single group (Ti,Nb)N, and even for this simple example of a mutually soluble system, an analytical solution could not be found. In addition to precipitate amounts, Figure 4 shows how the precipitate composition evolves with decreasing temperature. For example, at 1573 K (1300 °C), the precipitate group composition is 72 pct Ti, 6 pct Nb, and 22 pct N, which corresponds to the molar-fraction expression $Ti_{0.48}Nb_{0.02}N_{0.50}$. When titanium is present, TiN is the dominant precipitate at high temperature, owing to its high stability. Its molar fraction f_{TiN} decreases at lower temperature, as NbN forms from the remaining N and increases the Nb content of the precipitate. This result is consistent with experimental findings, such as those of Strid[69] and Craven,[70] where the core of complex carbonitrides is mainly TiN. The model suggests that precipitates generated at high temperature are Ti rich, and the precipitate layers that form later become richer in Nb as the temperature lowers. Figure 4(a) also shows results for the same steel without Ti. With mutual solubility, adding titanium remarkably increases the initial precipitation temperature and decreases the equilibrium activity of NbN, which allows more NbN to form. If TiN and NbN were mutually exclusive, then adding titanium would decrease NbN precipitation. This result illustrates the importance of proper consideration of mutual solubility in the model.

IV. MODEL VALIDATION

A. Validation with Commercial Package

The chemical composition of the two commercial steels in this work, 1004 LCAK (low carbon aluminum killed) and 1006Nb HSLA (high strength low alloy), are given in Table V. The results from the commercial package JMat-Pro 5.0 with general steel submodule[71] and the current model are compared in Figure 5. JMat-Pro predicts separate precipitation of a TiN-rich "MN" phase at higher temperatures and a NbC-rich "M(C,N)" phase at lower temperatures. These are treated together as a single (Ti,Nb,V)(C,N) phase with evolving composition in the current model, as previously mentioned. The oxide M_2O_3 predicted by JMat-Pro corresponds with the (Al,Ti)O phase in the current model.
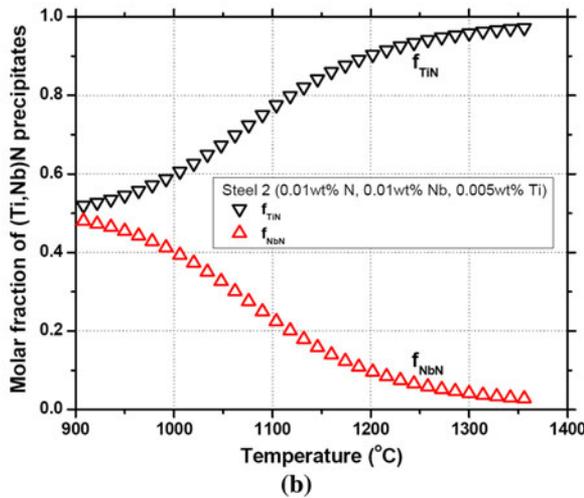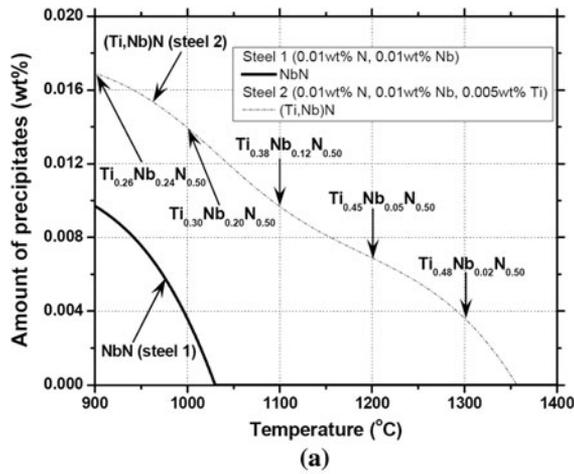
Fig. 4—Model calculation of mutually soluble precipitation in austenite for two Fe alloys containing 0.01 pct N and 0.01 pct Nb, with and without 0.005 pct Ti: (a) precipitate amount and (b) molar fraction of (Ti,Nb)N precipitates.
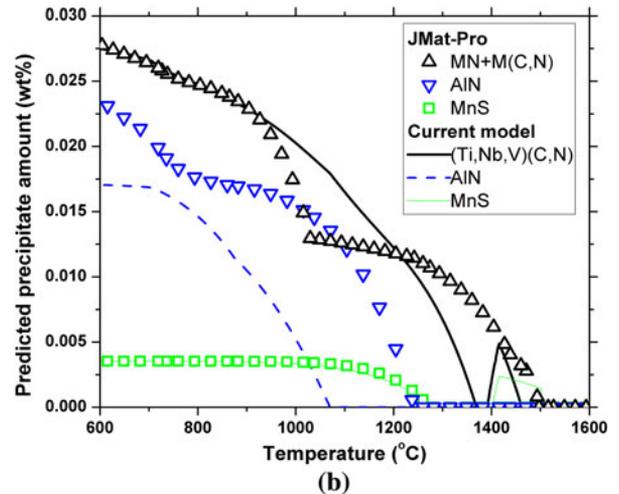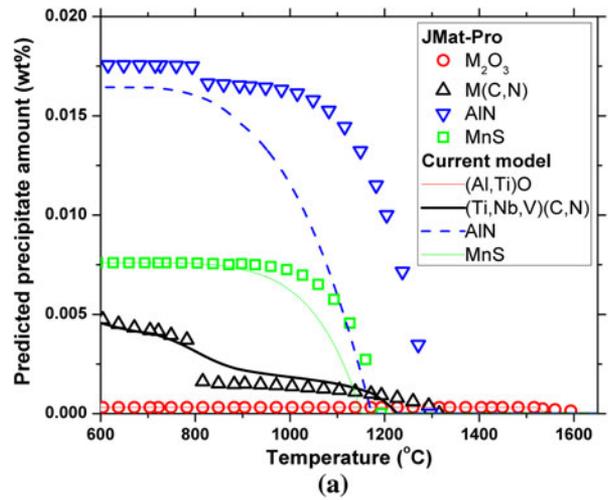

Fig. 5—Comparison of precipitate calculations by software JMat-Pro and the current model: (a) 1004 LCAK steel and (b) 1006Nb HSLA steel.

Table V. Compositions of 1004 LCAK and 1006Nb HSLA Steels (Weight Percent)

Steel	Al	C	Cr	Mn	Mo	N	Nb	S	Si	Ti	V	O
1004 LCAK	0.040	0.025	0.025	0.141	0.007	0.006	0.002	0.0028	0.028	0.0013	0.001	0.00015
1006Nb HSLA	0.0223	0.0472	0.0354	0.9737	0.0085	0.0083	0.0123	0.0013	0.2006	0.0084	0.0027	0

The comparison shows qualitative agreement for the predicted precipitate types, and the amounts of (Al, Ti,)O, MnS, and (Ti,Nb,V)(C,N) between the two models are all similar. For the latter phase group, JMat-Pro predicts a double-humped curve, owing to its two precipitate groups, MN and M(C,N), which is roughly approximated by a single smooth curve with the current model. The composition of (Ti,Nb,V)(C,N) in the current model also matches reasonably with the average composition of the two precipitate groups in JMat-Pro. For example, in 1006Nb steel, the calculated composition is $Ti_{0.48}Nb_{0.02}V_{0.00}C_{0.00}N_{0.50}$ at 1577 K (1304 °C) and $Ti_{0.28}Nb_{0.22}V_{0.00}C_{0.23}N_{0.27}$ at 1077 K

(804 °C) for JMat-Pro, and $Ti_{0.47}Nb_{0.03}V_{0.00}C_{0.02}N_{0.48}$ at 1577 K (1304 °C) and $Ti_{0.29}Nb_{0.21}V_{0.02}C_{0.14}N_{0.35}$ at 1077 K (804 °C) for the current model. The current model predicts that (Ti,Nb,V)(C,N) and MnS first form in the δ-ferrite phase, but dissolve after the transformation to austenite, where the solubilities are larger. This trend is missing in JMat-Pro. JMat-Pro consistently predicts more AlN than the current model, likely due to having less solubility for this precipitate in its database. Below 1073 K (800 °C), a jump in AlN is predicted by JMat-Pro. This is because cementite transformation is ignored in the current model. The carbon-rich Fe_3C phase provides plenty of carbon to allow MN and

Table VI. Compositions of Nb-Based Microalloyed Steels (Weight Percent)

Steel	C	Si	Mn	P	S	Nb	Al	N	V	Ti
Nb4	0.158	0.28	1.48	0.008	0.002	0.010	0.016	0.005	0.013	0.003
Nb8	0.081	0.31	1.44	0.010	0.002	0.033	0.017	0.004	0.011	0.003

M(C,N) to form nearly as pure carbide, which leaves more nitrogen to react with Al. In conclusion, the differences between the two models are not considered to be significant, considering that both models neglect the important effects of kinetics.

B. Validation with Measured Equilibrium-Precipitated Nb Amount

Zajac and Jansson[72] investigated equilibrium precipitation in several Nb-based industrial microalloyed steels, including the two compositions shown in Table VI. The steels were first solution treated at 1573 or 1623 K (1300 or 1350 °C) for 1 hour followed by quick water quenching. Then, specimens were aged at two different temperatures isothermally for 24 to

Fig. 6—Comparison of predicted amounts of Nb precipitation with experimental measurements at different temperatures (Table V steels[71]).

48 hours. The precipitated amount of Nb in Nb(C,N) was measured by the inductively coupled plasma emission method on electrolytically extracted compounds for each sample. Figure 6 compares these experimental measurements with the calculated results of the precipitated niobium amount for these two steels and shows that the current model matches well with the experimental data.

C. Validation with Observed Titanium Precipitate Types

Titanium sulfide and titanium carbosulfide are also observed in high-titanium steels. The equilibrium precipitation behavior of titanium-stabilized interstitial-free steels was studied quantitatively using dissolution experiments by Yang et al.[41] Several steels with different compositions were reheated at different temperatures varying from 1373 to 1623 K (1100 to 1350 °C), and the holding time to reach the equilibrium state varied from 1.5 to 3 hours for different reheating temperatures. The steel compositions and the types of precipitates observed at each holding temperature in the experiments are listed in Tables VII and VIII, respectively. The calculated molar fractions of the precipitates in these steels with temperature are shown in Figure 7. The model predictions are consistent with the observed stability of these precipitates. The oxide Al_2O_3 begins to form in the liquid steel, so was likely removed by the flux/slag and not recorded in the experiments.

D. Validation with Measured Inclusion Compositions for Welding

Inclusion formation in steel welds is important to decide the final microstructure and improve toughness in welds. It is also a good resource to validate the current model since many measurements are available in the literature. Kluken and Grong[73] measured the
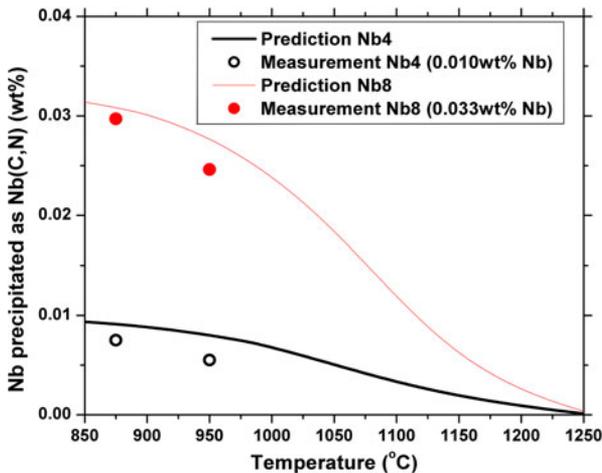
Table VII. Compositions of Ti-Based Microalloyed Steels (Weight Percent)

Steel	C	Si	Mn	P	S	Al	Ti	N	O
B	0.0036	0.0050	0.081	0.011	0.0028	0.045	0.095	0.0019	0.0028
C	0.0033	0.0040	0.081	0.011	0.0115	0.037	0.050	0.0022	0.0036

Table VIII. Precipitates Observed in Two Steels after Holding Several Hours at Different Temperatures

Steel	1300 °C	1250 °C	1200 °C	1150 °C	1100 °C
B	TiN	TiN, TiS*	TiN, TiS	TiN, $Ti_4C_2S_2$	TiN, $Ti_4C_2S_2$
C	TiN, TiS	TiN, TiS	TiN, TiS	TiN, TiS	TiN, <TiS>, $Ti_4C_2S_2$

*Very scarce.
< > Means minor amount.

inclusion compositions in term of average element concentrations of aluminum, titanium, manganese, silicon, sulfur, and copper in nine submerged arc welds with different steel compositions using the wavelength dispersive X-ray (EDX) intensity analysis and carbon extraction replicas method. The observed inclusions in the solidified weld pool consist of an oxide core forming due to reoxidation in the liquid state, and are covered partially by sulfides and nitrides on their surfaces. Simple empirical relations were suggested to compute the dissolved concentrations of alloying elements to match the measurements, and the order of precipitate formation was always Al_2O_3, Ti_2O_3, SiO_2, MnO, MnS, and TiN regardless of the weld composition.

Hsieh[74] used Thermo-Calc software to predict inclusion development in these low-alloy-steel welds. Multiphase equilibrium between oxides and liquid steel was assumed since the precipitation reactions are very fast at these high temperatures. The oxidation sequence was found to be sensitive to small changes in the weld composition. The calculation stopped at liquidus temperature 1800 K (1527 °C), so the possible formation of sulfides, nitrides, and carbides after solidification was not found.

The distributions of various precipitated compounds in the inclusions are computed by the current model as functions of steel composition. Since precipitates including copper are not considered in this study, the original measured inclusion composition data were normalized to make the sum of the mass concentration of aluminum, titanium, manganese, silicon, and sulfur total 100 pct, in order to allow for a proper comparison. The chemical compositions of the experimental welds are given in Table IX. A comparison of the calculated inclusion compositions at 1800 K (1527 °C) in liquid steel and 1523 K (1250 °C) in austenite with the measurements is shown in Figure 8, and reasonable agreement is found especially at 1523 K (1250 °C), after high-temperature solid-state reactions alter the normalized compositions, but before kinetics stops the diffusion (slope = 0.644 and correlation coefficient = 0.911 at 1800 K (1527 °C), and slope = 0.988 and correlation coefficient = 0.932 at 1523 K (1250 °C)). This finding indicates that the current model can be used as a first approximation to describe the formation of complex inclusions for different weld metal compositions. The agreement is likely adversely affected by the lack of consideration of kinetics and segregation during solidification in the current model.
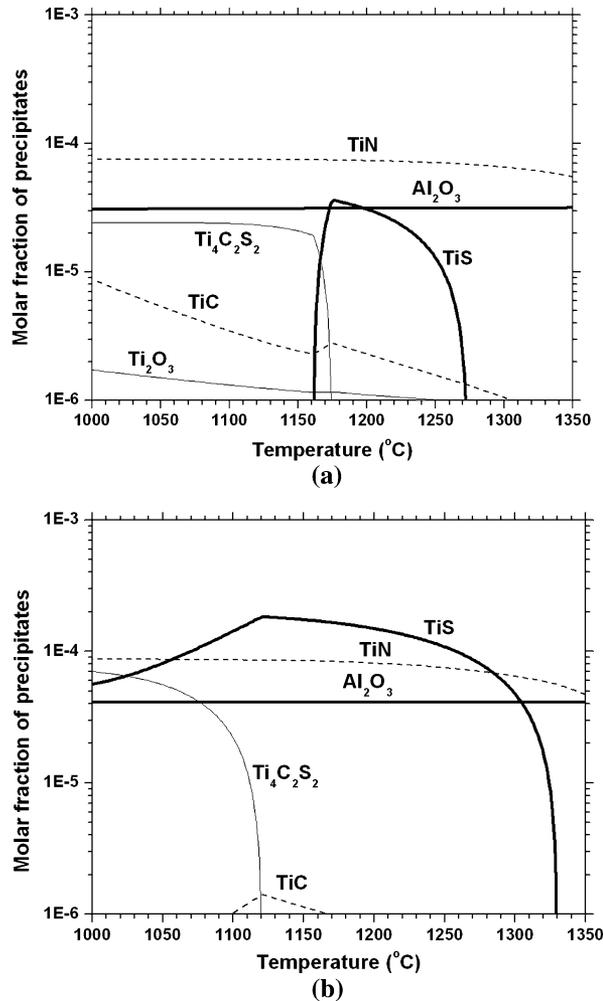
V. CALCULATION FOR COMMERCIAL STEELS IN CONTINUOUS CASTING

Temperature and phase fraction evolution during the solidification and cooling process is the first crucial step

Fig. 7—Calculated molar fractions of precipitates for Ti steels in Table VI: (a) steel B and (b) steel C.

Table IX. Compositions of Experimental Weld Steels (Weight Percent)

Weld	C	O	Si	Mn	P	S	N	Nb	V	Cu	B	Al	Ti
1	0.09	0.034	0.48	1.86	0.010	0.010	0.005	0.004	0.02	0.02	0.0005	0.018	0.005
2	0.09	0.037	0.55	1.84	0.010	0.009	0.005	0.005	0.02	0.03	0.0006	0.020	0.025
3	0.10	0.035	0.69	1.88	0.012	0.010	0.008	0.004	0.02	0.03	0.0008	0.028	0.063
4	0.10	0.030	0.52	1.87	0.010	0.007	0.005	0.007	0.01	0.06	0.0004	0.041	0.005
5	0.09	0.039	0.58	1.95	0.009	0.009	0.005	0.005	0.02	0.03	0.0006	0.037	0.022
6	0.09	0.040	0.69	1.97	0.009	0.009	0.006	0.007	0.02	0.03	0.0006	0.044	0.058
7	0.09	0.032	0.53	1.90	0.009	0.008	0.005	0.006	0.02	0.03	0.0004	0.062	0.008
8	0.10	0.031	0.62	1.92	0.010	0.010	0.005	0.005	0.02	0.03	0.0006	0.062	0.032
9	0.09	0.031	0.62	1.78	0.011	0.007	0.006	0.004	0.01	0.08	0.0006	0.053	0.053

Fig. 9—Evolution of phase fractions with temperature for 1004 LCAK and 1006Nb HSLA steels.

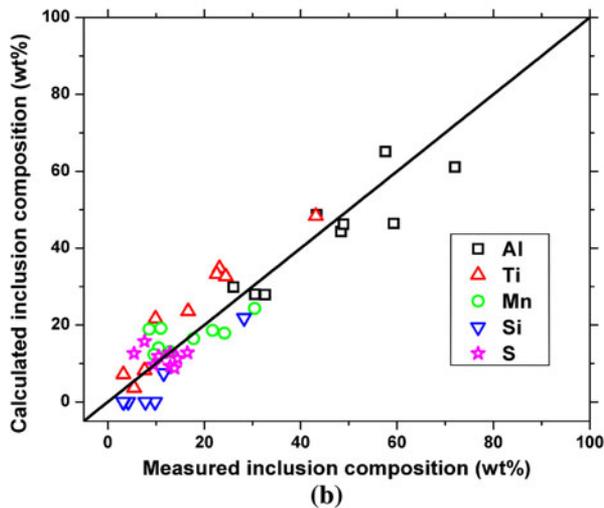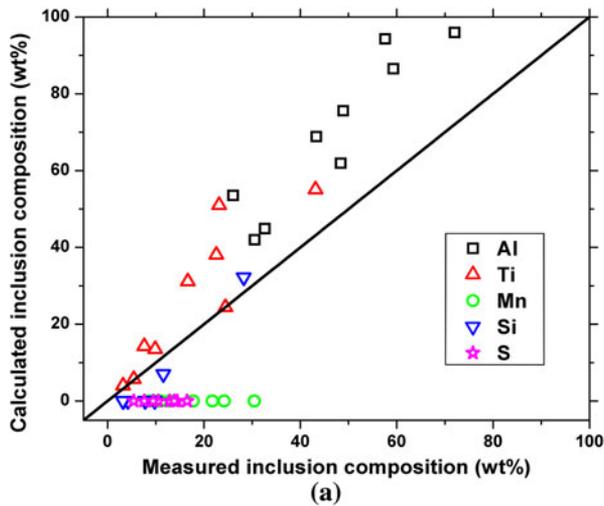Fig. 8—Comparison of calculated and measured inclusion compositions for welding metals:[72] (a) 1800 K (1527 °C) and (b) 1523 K (1250 °C).

to predict microstructure and ductility. In this study, the transient heat conduction equation is solved in the mold and spray regions of a continuous steel slab caster using the CON1D program.[75] This finite-difference model calculates one-dimensional heat transfer within the solidifying steel shell coupled with two-dimensional steady-state heat transfer in the mold and a careful treatment of the interfacial gap between the shell and mold. Below the mold, the model includes the temperature and spatially-dependent heat-transfer coefficients of each spray nozzle, according to the local water flow rates and the heat extraction into each support roll. A nonequilibrium microsegregation model, based on an analytical Clyne–Kurz equation developed by Won and Thomas,[76] was applied to compute the liquidus temperature, solidus temperature, and phase fractions.

The casting conditions are chosen to model two Nucor commercial low carbon steels, 1004 LCAK and 1006Nb HSLA, in a typical thin slab casting machine, with a 950-mm-long parallel mold. Details of the spray zone cooling conditions are given elsewhere.[77]
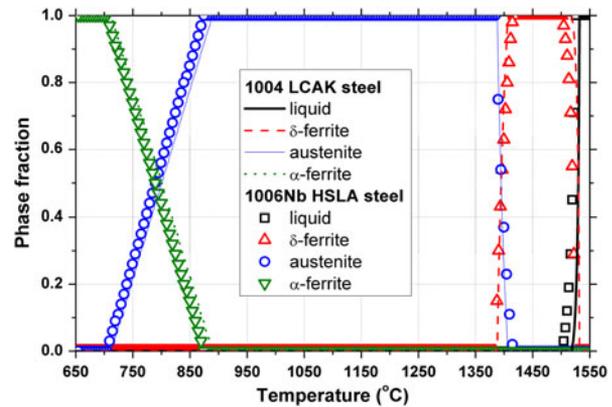
Simulations are run for a slab with 1396-mm width and 90-mm thickness. The pour temperature is 1826 K (1553 °C), and the casting speeds are 2.8 and 4.6 m/min. The water spray zones extend from the end of mold to 11.25 m below the meniscus. The chemical compositions of both steels are shown in Table V. The phase evolutions of 1004 LCAK and 1006Nb HSLA steels with temperature are shown in Figure 9, and small differences are found for the two steels. The calculated temperature and phase fraction histories at the slab surface are input to the current model for computing the corresponding equilibrium precipitation behaviors.

Figures 10(a) and (b) compare the predicted temperature and the predicted equilibrium precipitate phases of the two commercial steels with casting speed 2.8 m/min. It is seen that only precipitates (Ti,Nb,V)(C,N), MnS, and AlN form during casting for both steels, except that a small amount of oxides (Al,Ti)O exist from the liquid state for 1004 LCAK steel. The amounts of precipitates vary significantly due to the different steel compositions.

The influence of different casting speeds 2.8 and 4.6 m/min on the precipitation behavior of 1006Nb HSLA steel is shown in Figures 10(b) and (c). The higher casting speed causes higher surface temperature, for the same spray flow rates, and correspondingly less precipitates. TiN is the main precipitate at high temperature, especially in the mold, because of its lowest solubility limit. Precipitates of MnS and AlN then begin to form in succession. With the higher temperature of the high casting speed, AlN does not precipitate in the mold, and does not fully come out of solution until after exiting the caster (>15 m). This is significant because surface cracks often initiate in the mold due to strain concentration at the boundaries of locally enlarged grains, especially if they are embrittled by many fine precipitate particles.[78] Below the mold, thermal stresses in the spray-cooling zones and mechanical stresses from unbending can exacerbate surface cracking if precipitates are present. The results in Figure 10 explain why high casting speed may sometimes be beneficial in preventing these types of surface cracks.

It is important, however, to consider the kinetic effects, which are neglected in this model. Precipitation
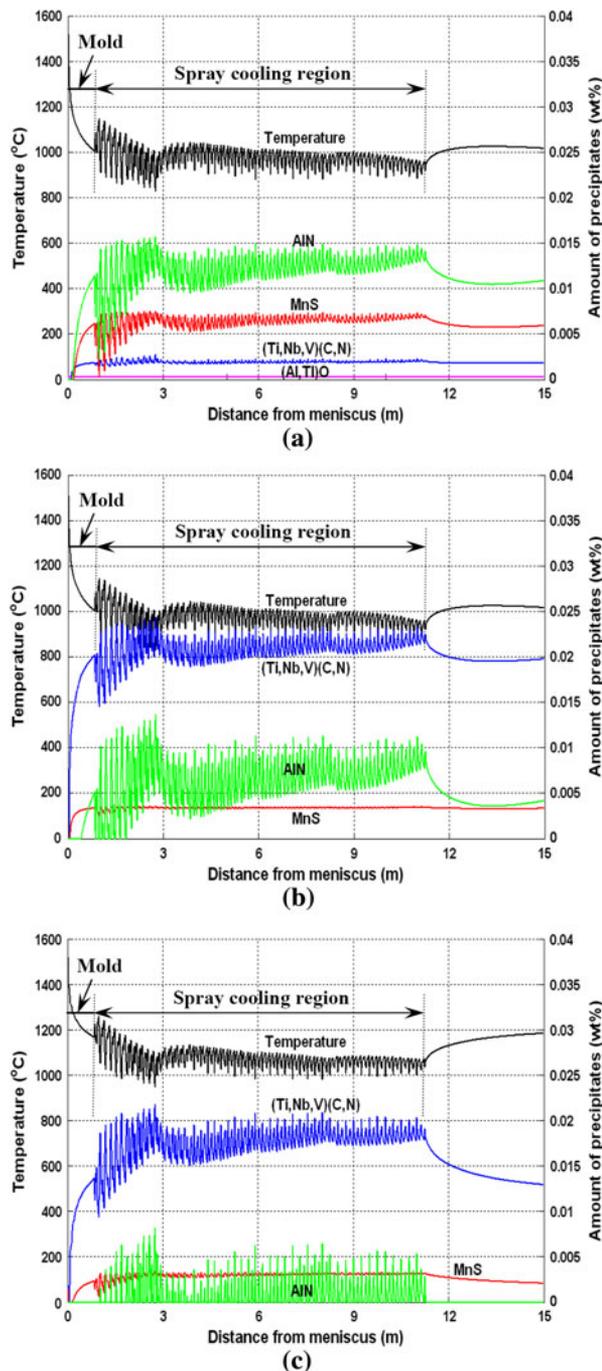
Fig. 10—Equilibrium precipitation behaviors of 1004 LCAK and 1006Nb HSLA steels in continuous casting with two different casting speeds: (*a*) 1004 LCAK steel with 2.8 m/min casting speed, (*b*) 1006Nb HSLA steel with 2.8 m/min casting speed, and (*c*) 1006Nb HSLA steel with 4.6 m/min casting speed.

is diffusion controlled and requires time to proceed, especially at lower temperature. The current model was used to simulate equilibrium precipitation on a similar thin-slab continuous caster for similar microalloyed Nb steel grades and somewhat overpredicted the measured precipitate amounts,[79] as expected, even after 15 minutes of reheating. This shows that this casting process is too fast to reach the equilibrium state shown in

Figure 10. Thus, the real precipitate amounts for these cases are expected to be lower and not to vary as much with the temperature oscillations in the spray zones. Considering the combined effects of shorter time and higher temperature, the drop in precipitation found in the 1006Nb HSLA steel, at the higher casting speed, should be more pronounced than that shown in Figure 10. Much more work is needed to make realistic predictions of precipitate formation during steel processing, including kinetic effects, and to further extend the models to gain insight into ductility and crack formation.

VI. SUMMARY AND CONCLUSIONS

A thermodynamic model is established to predict equilibrium precipitation behavior in microalloyed steels. This model calculates the solubility limit of 18 common precipitates including the Wagner interaction effect, mutual solubility effect, and complete mass conservation of all 13 alloying elements during precipitation. The model can predict the occurrence and stability of these common oxide, sulfide, nitride, and carbide precipitates in microalloyed steels, as well as their equilibrium compositions.

The impact of mutual solubility on precipitation is demonstrated. For mutually exclusive precipitates, the formation of a second precipitate phase may delay the formation and decrease the equilibrium amount of other precipitates when they share some alloying elements. However, this result tends to reverse for mutually soluble precipitates, because the mutual solubility decreases the equilibrium activities of these precipitates.

Precipitation diagrams constructed from the model results for a given temperature show how phase composition regions evolve. Starting from no precipitation at high temperature initially, precipitation begins for the most stable (least soluble) precipitates and increases with decreasing temperature, leading to overlapping phase regions where more than one precipitate can form at lower temperatures.

The model is validated with an analytical solution for simple cases involving mutually exclusive precipitates. It is further validated by comparison with the commercial package JMat-Pro. It is then validated by comparison with the measured amounts, types, and compositions of many different experimental results from previous literature. The current model matches reasonably well in all cases.

The precipitation behavior of commercial 1004 LCAK and 1006Nb HSLA steels in continuous casting with different casting speeds is calculated. TiN is the dominating precipitate in the mold because of its lowest solubility limit. The precipitates are mainly (Ti,Nb,V)(C,N), MnS, and AlN for both steels, but the amount of each precipitate varies greatly due to their steel composition differences. With higher casting speed for 1006Nb HSLA steel, higher temperature and less precipitates are obtained under the same spray flow and AlN does not precipitate in the mold.

In conclusion, an efficient solubility-product-based model of equilibrium precipitation in microalloyed steels

has been developed, which is easy to revise by adding new types of precipitates or to change the solubility data. Equilibrium models such as this one represent the first step in development of a comprehensive model of precipitate formation in steel. Future work will incorporate other important effects, such as segregation during solidification and kinetic effects that govern precipitate growth and size distribution.

REFERENCES

1. C. Zener (quoted by C.S. Smith): *Trans. AIME*, 1948, vol. 175, pp. 15–51.
2. J.A. Garrison, J.G. Speer, D.K. Matlock, and K.P. Williams: *AIST 2005 Proc.*, 2005, vol. II, pp. 107–16.
3. Y. Li, J.A. Wilson, D.N. Crowther, P. S. Mitchell, A.J. Craven, and T.N. Baker: *ISIJ Int.*, 2004, vol. 44, pp. 1093–1102.
4. M. Charleux, W.J. Poole, M. Militzer, and A. Deschamps: *Metall. Mater. Trans. A*, 2001, vol. 32A, pp. 1635–47.
5. M. Chapa, S.F. Medina, V. Lopez, and B. Fernandez: *ISIJ Int.*, 2002, vol. 42, pp. 1288–96.
6. S.C. Park, I.H. Jung, K.S. OH, and H.G. LEE: *ISIJ Int.*, 2004, vol. 44, pp. 1016–23.
7. B.G. Thomas, J.K. Brimacombe, and I.V. Samarasekera: *ISS Trans.*, 1986, vol. 7, pp. 7–20.
8. J.P. Michel and J.J. Jonas: *Acta Metall.*, 1981, vol. 29, pp. 513–26.
9. M. Hillert and L.I. Staffanson: *Acta Chem. Scand.*, 1970, vol. 24, pp. 3618–26.
10. B. Sundman and J. Agren: *J. Phys. Chem. Solids*, 1981, vol. 42, pp. 297–301.
11. N. Yoshinaga, K. Ushioda, S. Akamatsu, and O. Akisue: *ISIJ Int.*, 1994, vol. 34, pp. 24–32.
12. E.E. Kashif, K. Asakura, T. Koseki, and K. Shibata: *ISIJ Int.*, 2004, vol. 44, pp. 1568–75.
13. J.Y. Choi, B.S. Seong, S.C. Baik, and H.C. Lee: *ISIJ Int.*, 2002, vol. 42, pp. 889–93.
14. B.J. Lee: *Metall. Mater. Trans. A*, 2001, vol. 32A, pp. 2423–39.
15. M. Hillert, B. Jansson, B. Sundman, and J. Agren: *Metall. Trans. A*, 1985, vol. 16A, pp. 261–66.
16. Y. Sun and T. Bell: *Mater. Sci. Eng. A*, 1997, vol. 224, pp. 33–47.
17. H. Le Chatelier: *Annales des Mines, Hutieme Serie, Memiories*, Dunod, Paris, 1888, vol. XIII.
18. R.C. Hudd, A. Jones, and M.N. Kale: *J. Iron Steel Inst.*, 1971, vol. 209, pp. 121–25.
19. T. Gladman: *The Physical Metallurgy of Microalloyed Steels*, The Institute of Materials, London, 1997, pp. 82–130.
20. W.J. Liu and J.J. Jonas: *Metall. Trans. A*, 1989, vol. 20A, pp. 1361–74.
21. N. Gao and T.N. Baker: *ISIJ Int.*, 1997, vol. 37, pp. 596–604.
22. H. Adrian: *Mater. Sci. Technol.*, 1992, vol. 8, pp. 406–20.
23. P.R. Rios: *Mater. Sci. Eng.*, 1992, vol. A156, pp. L5–L8.
24. J.Y. Park, J.K. Park, and W.Y. Choo: *ISIJ Int.*, 2000, vol. 40, pp. 1253–59.
25. G.V. Pervushin and H. Suito: *ISIJ Int.*, 2001, vol. 41, pp. 748–56.
26. K. Nakajima, H. Hasegawa, S. Khumkoa, and S. Mizoguchi: *Metall. Mater. Trans. B*, 2003, vol. 34B, pp. 539–47.
27. R.L. Clendenen and H.G. Drickamer: *J. Chem. Phys.*, 1966, vol. 44, pp. 4223–28.
28. J.C. Brick: *J. Mater. Sci.*, 1980, vol. 15, pp. 161–67.
29. S.P. Farrell, M.E. Fleet, I.E. Stekhin, A. Kravtsova, A.V. Soldatov, and X. Liu: *Am. Mineral.*, 2002, vol. 87, pp. 1321–32.
30. M. Hua, C.I. Garcia, and A.J. DeArdo: *Scripta Metall. Mater.*, 1993, vol. 28, pp. 973–78.
31. A.V. Kurdyumov, V.L. Solozhenko, and W.B. Zelyavski: *J. Appl. Crystallogr.*, 1995, vol. 28, pp. 540–45.
32. D. Sundararaman, P. Shankar, and V.S. Raghunathan: *Metall. Mater. Trans. A*, 1996, vol. 27A, pp. 1175–86.
33. *Steelmaking Data Sourcebook*, The Japanese Society for the Promotion of Science, The 19th Committee on Steelmaking (revised edition), Gordon and Breach Science Publishers, New York, 1988, pp. 45, 169.
34. T. Binran: *Iron and Steel Handbook*, 3rd ed., ISIJ, ed., Maruzen Co. Ltd., Tokyo, 1981, vol. 1, p. 15.
35. H. Itoh, M. Hino, and S. Ban-ya: *ISIJ*, 1997, vol. 83, pp. 623–28.
36. S. Dimitrov, A. Weyl, and D. Janke: *Steel Res.*, 1995, vol. 66, pp. 87–92.
37. E.T. Turkdogan: *Fundamental of Steelmaking*, The Institute of Materials, London, 1996, p. 128.
38. K. Inonu, I. Ohnuma, H. Ohtani, K. Ishida, and T. Nishizawa: *ISIJ Int.*, 1998, vol. 38, pp. 991–97.
39. E.T. Turkdogan, S. Ignatowicz, and J. Pearson: *J. Iron Steel Inst.*, 1955, vol. 180, pp. 349–54.
40. J. Yang, K. Okumura, M. Kuwabara, and M. Sano: *ISIJ Int.*, 2002, vol. 42, pp. 685–93.
41. X. Yang, D. Vanderschueren, J. Dilewijns, C. Standaert, and Y. Houbaert: *ISIJ Int.*, 1996, vol. 36, pp. 1286–94.
42. V. Beta and E.V. Pereloma: *Scripta Mater.*, 2005, vol. 53, pp. 141–43.
43. M. Hillert and M. Jarl: *Metall. Trans. A*, 1975, vol. 6A, pp. 553–59.
44. S. Ban-ya, J.F. Elliott, and J. Chipman: *Metall. Trans.*, 1970, vol. 1, pp. 1313–20.
45. W.J. Liu, J.J. Jonas, D. Bouchard, and C.W. Bale: *ISIJ Int.*, 1990, vol. 30, pp. 985–90.
46. V.K. Lakshmanan: M. Eng. Thesis, McMaster University, Hamilton, ON, Canada.
47. Z. Morita and K. Kunisada: *ISIJ*, 1977, vol. 63, pp. 1663–71.
48. Y.M. Pomarin, G.M. Grigorenko, and V.I. Lakomakii: *Russ. Metall.*, 1975, No. 5, pp. 61–65.
49. D.B. Evans and R.D. Pehlke: *Trans. TMS-AIME*, 1965, vol. 233, pp. 1620–24.
50. G.K. Sigworth and J.F. Elliott: *Met. Sci.*, 1974, vol. 8, pp. 298–310.
51. M. Jarl: *Scand. J. Metall.*, 1978, vol. 7, pp. 93–101.
52. J. Pak, J. Yoo, Y. Jeong, S. Tae, S. Seo, D. Kim, and Y. Lee: *ISIJ Int.*, 2005, vol. 45, pp. 23–29.
53. D.B. Evans and R.D. Pehlke: *Trans. TMS-AIME*, 1964, vol. 230, pp. 1657–62.
54. R.C. Sharma, V.K. Lakshmanan, and J.S. Kirkaldy: *Metall. Trans. A*, 1984, vol. 15A, pp. 545–53.
55. T. Wada, H. Wada, J.F. Elliott, and J. Chipman: *Metall. Trans.*, 1972, vol. 3, pp. 1657–67.
56. T. Wada, H. Wada, J.F. Elliott, and J. Chipman: *Metall. Trans.*, 1972, vol. 3, pp. 2865–72.
57. M. Kishi, R. Inoue, and H. Suito: *ISIJ Int.*, 1994, vol. 34, pp. 859–67.
58. Y. Guo and C. Wang: *Metall. Trans. B*, 1990, vol. 21B, pp. 543–47.
59. Q. Han: *Proc. 6th Int. Iron Steel Congr.*, ISIJ, Tokyo, 1990, vol. 1, pp. 166–76.
60. Z Morita, T. Tanaka, and T. Yanai: *Metall. Trans. B*, 1987, vol. 18B, pp. 195–202.
61. Z. Hong, X. Wu, and C. Kun: *Steel Res.*, 1995, vol. 66, pp. 72–76.
62. S. Jo, B. Song, and S. Kim: *Metall. Mater. Trans. B*, 2002, vol. 33B, pp. 703–09.
63. S. Abraham, R. Klein, R. Bodnar, and O. Dremailova: *Materials Science Technology*, (MS&T) Conf, TMS, Warrendale, PA, 2006, pp. 109–22.
64. R.C. Nunnington and N. Sutcliffe: *59th Electric Furnace Conf. Proc.*, Phoenix, AZ 2001, ISS, Warrendale, PA, 2002, vol. 84, pp. 361–94.
65. C. Wagner: *Thermodynamics of Alloys*, Addison-Wesley Publishing Company, Cambridge, MA, 1952, pp. 51–53.
66. J. Chipman: *J. Iron Steel Inst.*, 1955, vol. 180, pp. 97–103.
67. C.H.P. Lupis and J.F. Elliott: *Acta Metall.*, 1966, vol. 14, pp. 526–31.
68. J.G. Speer, J.R. Michael, and S.S. Hansen: *Metall. Trans. A*, 1987, vol. 18A, pp. 211–22.
69. J. Strid and K.E. Easterling: *Acta Metall.*, 1985, vol. 33, pp. 2057–74.
70. A.J. Craven, K. He, L.A.J. Craven, and T.N. Baker: *Acta Mater.*, 2000, vol. 48, pp. 3857–68.
71. *JMat Pro (Materials Property Simulation Package Public Release Version 5.0)*, Sente Software, Guildford, United Kingdom, 2010.
72. S. Zajac and B. Jansson: *Metall. Mater. Trans. B*, 1998, vol. 29B, pp. 163–76.

73. A.O. Kluken and Ø. Grong: *Metall. Trans. A*, 1989, vol. 20A, pp. 1335–49.
74. K.C. Hsieh, S.S. Babu, J.M. Vitek, and S.A. David: *Mater. Sci. Eng. A*, 1996, vol. 215, pp. 84–91.
75. Y. Meng and B.G. Thomas: *Metall. Mater. Trans. B*, 2003, vol. 34B, pp. 685–705.
76. Y.M. Won and B.G. Thomas: *Metall. Mater. Trans. A*, 2001, vol. 32A, pp. 1755–67.
77. K. Zheng, B. Petrus, B.G. Thomas, and J. Bentsman: *AISTech 2007 Conf. Proc.*, Indianapolis, IN, 2007, vol. 2, pp. 165–79.
78. E.S. Szekeres: *Proc. 6th Int. Conf. on Clean Steel*, Balatonfüred, Hungary, June 2002, pp. 324–38.
79. S. Dyer, J.G. Speer, D.K. Matlock, A.J. Shutts, S. Jansto, K. Xu, B.G. Thomas: *Iron Steel Tech.*, 2010, pp. 96–105 (reprinted from *AISTech 2010*, Pittsburgh, PA).